



## RESEARCH ARTICLE

## OPEN ACCESS

# Noninvasive Grading of Liver Fibrosis Based on Texture Analysis From MRI-Derived Radiomics

Jennifer Gotta<sup>1</sup> | Leon D. Gruenewald<sup>1</sup> | Philipp Reschke<sup>1</sup> | Christian Booz<sup>1</sup> | Scherwin Mahmoudi<sup>1</sup> | Bram Stieltjes<sup>2</sup> | Moon Hyung Choi<sup>3</sup> | Tommaso D'Angelo<sup>4</sup> | Simon Bernatz<sup>1</sup> | Thomas J. Vogl<sup>1</sup> | Ralph Sinkus<sup>5</sup>  | Robert Grimm<sup>6</sup> | Ralph Strecker<sup>7</sup> | Sebastian Haberkorn<sup>8</sup> | Vitali Koch<sup>1</sup> 

<sup>1</sup>Department of Radiology, Goethe University Hospital Frankfurt, Frankfurt am Main, Germany | <sup>2</sup>Department of Radiology, Universitätsspital Basel, Basel, Switzerland | <sup>3</sup>Department of Radiology, Eunpyeong St Mary's Hospital, College of Medicine, The Catholic University of Korea, Seoul, Republic of Korea | <sup>4</sup>Department of Biomedical Sciences and Morphological and Functional Imaging, University Hospital Messina, Messina, Italy | <sup>5</sup>Laboratory of Translational Vascular Sciences, U1148, INSERM, Université de Paris, Paris, France | <sup>6</sup>MR Application Predevelopment, Siemens Healthcare GmbH, Erlangen, Germany | <sup>7</sup>EMEA Scientific Partnerships, Siemens Healthcare GmbH, Forchheim, Germany | <sup>8</sup>Department of Cardiology, Goethe University Hospital Frankfurt, Frankfurt am Main, Germany

**Correspondence:** Jennifer Gotta ([jennifer.gotta@unimedizin-ffm.de](mailto:jennifer.gotta@unimedizin-ffm.de))

**Received:** 25 October 2024 | **Revised:** 14 November 2024 | **Accepted:** 15 November 2024

**Funding:** The authors received no specific funding for this work.

**Keywords:** liver cirrhosis | liver fibrosis | magnetic resonance imaging | radiomics

## ABSTRACT

Given the increasing global prevalence of metabolic syndrome, this study aimed to assess the potential of MRI-derived radiomics in noninvasively grading fibrosis. The study included 79 prospectively enrolled participants who had undergone MRE due to known or suspected liver disease between November 2022 and September 2023. Among them, 48 patients were diagnosed with histopathologically confirmed liver fibrosis. A total of 107 radiomic features per patient were extracted from MRI imaging. The dataset was then divided into training and test sets for model development and validation. Stepwise feature reduction was employed to identify the most relevant features and subsequently used to train a gradient-boosted tree model. The gradient-boosted tree model, trained on the training cohort with identified radiomic features to differentiate fibrosis grades, exhibited good performances, achieving AUC values from 0.997 to 0.998. In the independent test cohort of 24 patients, the radiomics model demonstrated AUC values ranging from 0.617 to 0.830, with the highest AUC of 0.830 (95% CI 0.520–0.830) for classifying fibrosis grade 2. Incorporating ADC values did not improve the model's performance. In conclusion, our study emphasizes the significant promise of using radiomics analysis on MRI images for noninvasively staging liver fibrosis. This method provides valuable insights into tissue characteristics and patterns, enabling a retrospective liver fibrosis severity assessment from nondedicated MRI scans.

## 1 | Introduction

Metabolic dysfunction-associated steatotic liver disease (MASLD) represents a growing global health concern with a high prevalence and the associated risk of inflammation,

progressive liver fibrosis, cirrhosis, and finally, hepatocellular carcinoma [1, 2].

MASLD has seen a drastic increase in both incidence and prevalence over the past three decades, emerging as the leading

**Abbreviations:** ADC, apparent diffusion coefficient; AUC, area under the curve; GLCM, gray-level co-occurrence matrix; GLDM, gray-level dependence matrix; GLRLM, gray-level run length matrix; GLSZM, gray-level size zone matrix; LF, liver fibrosis; MASH, metabolic dysfunction-associated steatohepatitis; MASLD, metabolic dysfunction-associated steatotic liver disease; ML, machine learning; MRE, magnetic resonance elastography; MRI, magnetic resonance imaging; NGTDM, neighboring gray tone difference matrix; ROC, receiver operating characteristic; ROI, region of interest; SD, standard deviation.

This is an open access article under the terms of the [Creative Commons Attribution-NonCommercial](https://creativecommons.org/licenses/by-nc/4.0/) License, which permits use, distribution and reproduction in any medium, provided the original work is properly cited and is not used for commercial purposes.

© 2024 The Author(s). *NMR in Biomedicine* published by John Wiley & Sons Ltd.

cause of end-stage liver disease globally [3–5]. This upward trend is anticipated to continue, driven by societal and dietary changes expected to exacerbate the burden on healthcare systems [6]. MASLD often presents with no or mild symptoms in the early stages, making early detection challenging. However, the disease can progress from simple steatosis to metabolic dysfunction-associated steatohepatitis (MASH) with fibrosis and, ultimately, liver cirrhosis [7].

This gradual progression underscores the need for early identification and evaluation of patients. Interventions such as lifestyle and dietary modifications are most effective during the early stages of the disease, offering a window of opportunity to prevent more severe outcomes. As new therapeutic strategies emerge, noninvasive methods to assess treatment efficacy and monitor disease progression become increasingly important [8–11].

Traditional diagnostic methods, particularly liver biopsy, offer valuable insights into the severity of fibrosis [12, 13]. However, their invasive nature and frequently false negative results underscore the need to explore noninvasive alternatives. Recent advancements in medical imaging present a promising pathway to acquire more detailed tissue information [14]. The integration of machine learning (ML), a subset of artificial intelligence, empowers computers to discern patterns and make predictions without explicit programming autonomously. Coupled with radiomics, a quantitative analysis designed to extract texture features from medical imaging that are not visually assessable, this integration holds significant promise in enhancing liver fibrosis assessment using magnetic resonance imaging (MRI) scans [14, 15].

Therefore, this study aimed to evaluate the potential of MRI-derived radiomics for noninvasive fibrosis grading with the goal of providing a reliable alternative for assessing fibrosis in patients with suspected liver disease.

## 2 | Methods

### 2.1 | Study Population

In this study, we compiled clinical data and MRI datasets from 79 prospectively enrolled patients with known or suspected liver disease who had undergone MR elastography (MRE) scans together with a standardized MRI protocol from routine clinical practices between November 2022 and September 2023 [16].

Inclusion criteria comprised patients aged over 18 years with histologically confirmed fibrosis. Additionally, healthy volunteers with no known abdominal or liver diseases were included as a control group. None of these healthy volunteers had undergone a liver biopsy, thus, a fibrosis stage of F0 was assumed.

Medical reports provided the primary data source and additional patient information and parameters were extracted from electronic patient files. According to the Metavir fibrosis staging system [17], liver fibrosis (LF) stages were categorized as follows: fibrosis grade 0, absence of fibrosis; fibrosis grade 1, presence of portal fibrosis; fibrosis grade 2, presence of periportal fibrosis; fibrosis grade 3, presence of septal fibrosis; and fibrosis grade 4, presence of cirrhosis.

Exclusion criteria encompassed no biopsy-proven fibrosis results, the inability to undergo MRI (e.g., claustrophobia, metallic implants or pregnancy), or insufficient image quality. The study design is shown in Figure 1.

The local ethical committee granted approval for this study and the research was conducted in adherence to these guidelines. All analyses were performed in compliance with local data protection regulations.

### 2.2 | MRI Scan Protocol

MRI was conducted on a 1.5 T MR scanner (MAGNETOM Aera, Siemens Healthineers, Erlangen, Germany). The complete clinical MR protocol included anatomical fat-saturated T1-weighted 3D gradient-echo Dixon VIBE (volumetric interpolated breath-hold examination), T2-weighted 2D turbo spin-echo, and diffusion-weighted 2D sequences, all part of the department's standard liver imaging protocol (Table S2).

### 2.3 | Image Segmentation Process

After anonymization, all patients' MRI datasets were extracted as Digital Imaging and Communications in Medicine (DICOM) datasets and then uploaded into the MR Liver Analysis Research Application (Siemens Healthineers). Each patient's liver segmentation process was automatically performed at the T1-weighted 3D gradient-echo Dixon VIBE sequence and the resulting segmentation file was uploaded to 3D Slicer (Version 5.0.2, Harvard University, Cambridge, USA). An illustrative example of the segmentation is provided in Figure 2. Experienced radiologists with up to 11 years of experience in abdominal imaging evaluated the segmentation in each case. When there was any disagreement with the initial segmentation, the process was repeated by an additional abdominal radiologist in this field and necessary adjustments were made. Notably, all participating radiologists in the assessment were unaware of the patients' clinical data.

### 2.4 | Extraction of Radiomics Features

Radiomics features were obtained using the PyRadiomics extension package within the 3D Slicer software (Version 5.1.0; 2022-05-20). The extraction process yielded 107 features for each segmentation (Table S1) [18]. These features were subsequently categorized into seven distinct groups, namely, gray-level dependence matrix (GLDM), gray-level co-occurrence matrix (GLCM), gray-level run length matrix (GLRLM), gray-level size zone matrix (GLSZM), neighboring gray tone difference matrix (NGTDM), shape, and first order [18]. To comprehensively evaluate the transparency and quality of the study, we incorporated a CheckList for Evaluation of Radiomics Research (CLEAR) into Figure S1 [19].

### 2.5 | Radiomics Feature Selection

A multistep feature selection methodology was implemented to identify the most pertinent features for subsequent

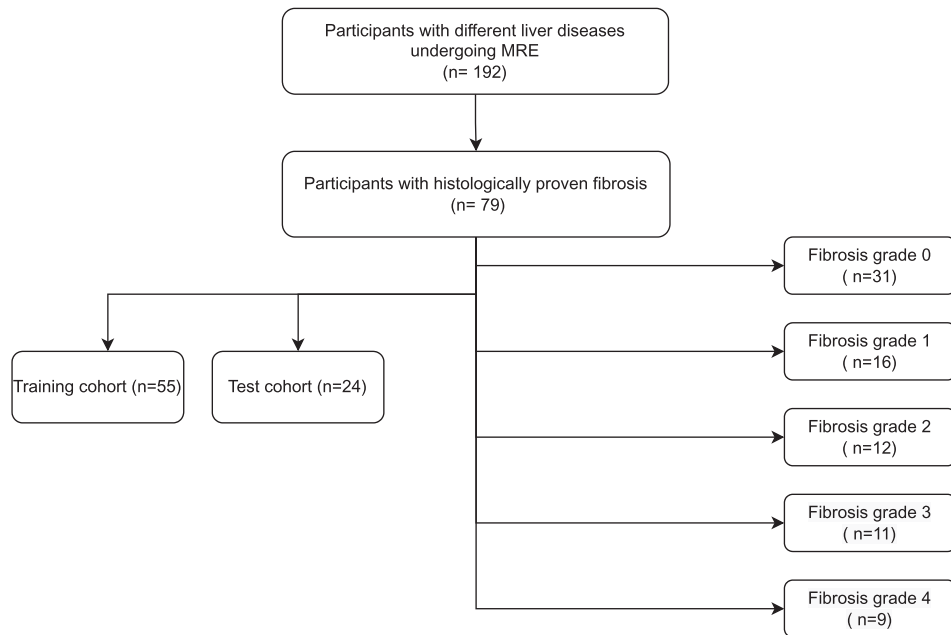


**FIGURE 1** | Flowchart of patient inclusion. MRE, magnetic resonance elastography. Note that this study includes a subset of a previously reported study population.

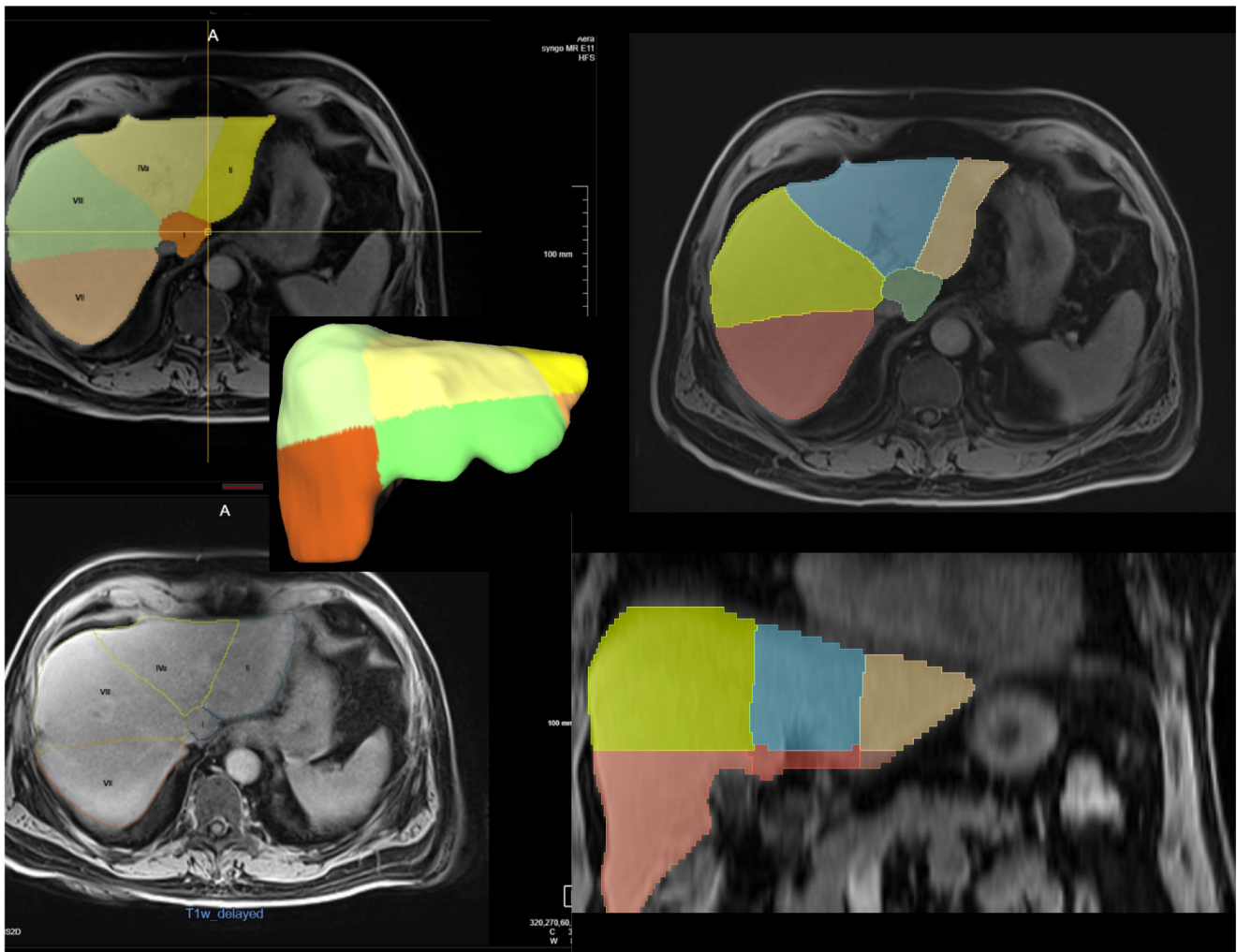


**FIGURE 2** | Exemplary segmentation of the liver. Left side: segmentation of the liver using MR Liver Analysis Research Application (Siemens Healthineers, Forchheim, Germany). Right side: transfer of the segmentation into 3D-Slicer (Version 5.0.2, Harvard University, Cambridge, USA).

analysis. Initially, all numerical features underwent normalization through Z-score standardization. Following this, the Boruta dimension reduction and feature elimination algorithm were employed [20]. Additionally, a correlation analysis was executed to detect clusters of features with high correlation, delineated by a Pearson's correlation coefficient ( $r \geq 0.60$ ). A feature with the highest Gini index was chosen from each cluster for further analysis.

## 2.6 | Construction of the Radiomics Model

The development of the radiomics model involved training a gradient-boosted tree model on the chosen radiomic features to distinguish between the different fibrosis grades, utilizing a training dataset that included 55 patients. The model's performance was then evaluated using a separate test dataset consisting of 24 patients. This test dataset had not previously been included in the model's training phase. The dataset was randomly divided into training and test sets.

## 2.7 | Statistical Analysis

Statistical analysis was performed using R statistical software (R Foundation for Statistical Computing, Vienna, Austria; Version 2023.06.0 + 421) and MedCalc (MedCalc Software Ltd., Ostend, Belgium; Version 20.123). Normally distributed data were presented as mean  $\pm$  standard deviation (SD), while nonnormally distributed data were reported as median and interquartile range (IQR). The *t*-test was utilized for normally distributed continuous variables, while the Mann–Whitney test or Spearman rank correlation coefficient was employed for nonnormally distributed variables.

Receiver operating characteristic (ROC) curve analyses were conducted to evaluate the performance of the radiomics model. A significance level below 0.05 was considered statistically significant.

# 3 | Results

## 3.1 | Patient Characteristics

Data from 79 participants with a mean age of 55 years ( $\pm 15$  years) were analyzed in this study. The cohort included 41 male (52%) and 38 female (48%) participants. Among these, 48 with histologically proven fibrosis of the liver were included. The comparative group with no liver fibrosis consisted of 31 patients. The predominant fibrosis grade identified in the study was grade 1, observed in 20% of cases, with grade 2 following at 15%. Table 1 presents a summary of sociodemographic and clinical characteristics.

## 3.2 | Selection of Radiomics Features

Initially, 107 features were extracted from the MRI datasets. After implementing the Boruta feature reduction algorithm, 13 features were identified as crucial for analysis. A correlation matrix was also generated to identify clusters of highly correlated

features, facilitating further feature reduction. Figure 3 illustrates the correlation matrix, emphasizing the key features for distinguishing between the different fibrosis grades. After the feature reduction process, eight features were retained for analysis. Table 2 presents the most relevant features identified through this multistep selection process.

## 3.3 | Performance of the Radiomics Model in the Training Cohort

The gradient-boosted tree model trained on the training cohort, utilizing the identified radiomic features to distinguish between different fibrosis grades, demonstrated excellent performance, achieving AUC values ranging from 0.997 (95% CI 0.991–0.997) to 1.0 (95% CI 1.0–1.0) in diagnosing the various fibrosis grades. Performance metrics for the training cohort are presented in Table 3.

## 3.4 | Performance of the Radiomics Model in the Test Cohort

The model's generalization capability was evaluated on an independent test cohort of 24 patients. The radiomics model achieved AUC values from 0.617 to 0.830 in the test cohort, with the highest AUC of 0.830 (95% CI 0.520–0.830) for classifying fibrosis grade 2 (Figure 4).

## 3.5 | Performance of the Radiomics Model Adding Apparent Diffusion Coefficient (ADC) Values

A subanalysis examining the impact of adding ADC to radiomics models for predicting fibrosis grades generally revealed a decrease in model performance, as indicated by lower AUC values when compared to radiomics alone. For fibrosis grade 2, the radiomics model achieved the highest AUC of 0.830, while the combination with ADC reduced the AUC to 0.694. Only for fibrosis grade 3 did the addition of ADC result in a slight improvement, increasing the AUC from 0.610 to 0.700. However, all changes in AUC values were not statistically significant ( $p > 0.05$ ).

# 4 | Discussion

The prevalence of MASLD is increasing globally, with the potential to advance from isolated steatosis to MASH. This progression poses serious risks, including conditions like cirrhosis, hepatocellular carcinoma or even mortality [21]. Therefore, accurate assessment and monitoring of liver fibrosis will become increasingly essential tasks in routine clinical practice. Even in the absence of significant symptoms during the initial phases, there is a gradual advancement from simple steatosis to MASH, accompanied by fibrosis and ultimately leading to liver cirrhosis [22]. An accurate and early diagnosis is important for detecting patients in the early stages, when lifestyle and dietary changes can be most beneficial [8]. With the development of new therapeutic strategies, noninvasive methods for evaluating treatment effectiveness and tracking disease progression will become increasingly important [9].

**TABLE 1** | Baseline characteristics of the study population.

Variables <i>n</i> (%) or mean (SD) or median (interquartile range)	Full sample ( <i>n</i> = 79)	Training cohort ( <i>n</i> = 55)	Test cohort ( <i>n</i> = 24)
<b>Demographics</b>			
Overall age (years)	58 (20–82)	58 (44–82)	58 (20–65)
Male sex ( <i>n</i> )	41(52%)	25(45%)	16 (66%)
Female sex ( <i>n</i> )	38 (48%)	30(55%)	8 (33%)
<b>Fibrosis grade</b>			
0	31 (39%)	24 (44%)	7 (29%)
1	16 (20%)	10 (18%)	6 (25%)
2	12 (15%)	10 (18%)	2 (8%)
3	11 (14%)	6 (11%)	5 (21%)
4	9 (11%)	5 (9%)	4 (17%)
<b>Laboratory parameters</b>			
GPT(U/L)	42.0 (6.0–936.0)	45.0 (26.0–78.3)	34.0 (21.0–64.5)
GOT (U/L)	39.5 (13.0–849.0)	38.5 (27.0–57.8)	44.5 (28.0–58.0)
De Ritis ratio	0.9 (0–9.1)	0.9 (0.6–1.3)	1.2 (0.8–1.5)
yGT (U/L)	82.5 (8.0–1312.0)	87.5 (41.25–166.0)	74.0 (36.5–174.2)
Alkaline phosphatase (U/L)	102.0 (39.0–986.0)	92.5 (70.5–132.5)	128.0 (100.0–199.0)
LDH (U/L)	219.0 (175.0–605.0)	217.0 (199.5–275.0)	228.0 (209.0–286.0)
<b>Risk factors</b>			
Obesity ( <i>n</i> )	50 (63%)	38 (69%)	12 (50%)
BMI (kg/m <sup>2</sup> )	29.8 (26.6–31.5)	26.8 (26.6–29.8)	31.0 (29.3–31.5)
Diabetes mellitus ( <i>n</i> )	21 (27%)	15 (27%)	6 (25%)
Arterial hypertension ( <i>n</i> )	22 (28%)	16 (29%)	6 (25%)
Current smoking ( <i>n</i> )	18 (23%)	16 (29%)	2 (8%)
Hypercholesterinemia ( <i>n</i> )	51 (65%)	37 (67%)	14 (58%)

Abbreviations: BMI, body mass index; GOT, glutamate-oxaloacetate transaminase; GPT, glutamate-pyruvate transaminase; LDH, lactate dehydrogenase; yGT, gamma-glutamyltransferase.

Although liver biopsy continues to be regarded as the gold standard for evaluating liver fibrosis, its extensive application is hindered by potential complications and its associated costs. Various MRI-based methods have emerged as noninvasive alternatives for staging liver fibrosis [23, 24], among which MRE currently presents the most promising noninvasive method [25, 26]. MRE and ultrasound-based elastography stand out as extensively validated techniques in clinical practice [26]. However, these elastography methods necessitate specialized scanners or additional equipment and may encounter challenges in patients with ascites or severe obesity. Moreover, the reliability of these techniques may be compromised due to the variability in radiologists' region of interest (ROI) selection. In contrast, the ML model offers a significant advantage in its broad applicability to routine CT or MRI images, characterized by high reproducibility and widespread availability.

In many medical fields, there is increasing interest in integrating machine learning into diverse healthcare domains to alleviate physician workload and streamline diagnostic processes [27, 28]. ML offers an advantage in handling extensive, complex, and diverse datasets, allowing it to automatically process large volumes of data. Over the past decade, increasing evidence has underscored the importance of incorporating quantitative imaging biomarkers into established clinical decision-making frameworks. This integration facilitates the automated extraction of valuable imaging features for diagnosing a range of medical conditions or obtaining tissue information [29, 30]. One major advantage is the retrospective assessment of MRI scans done for other reasons, for example, cancer staging.

In this context, radiomics is a quantitative method that allows for extracting texture features from medical imaging data that



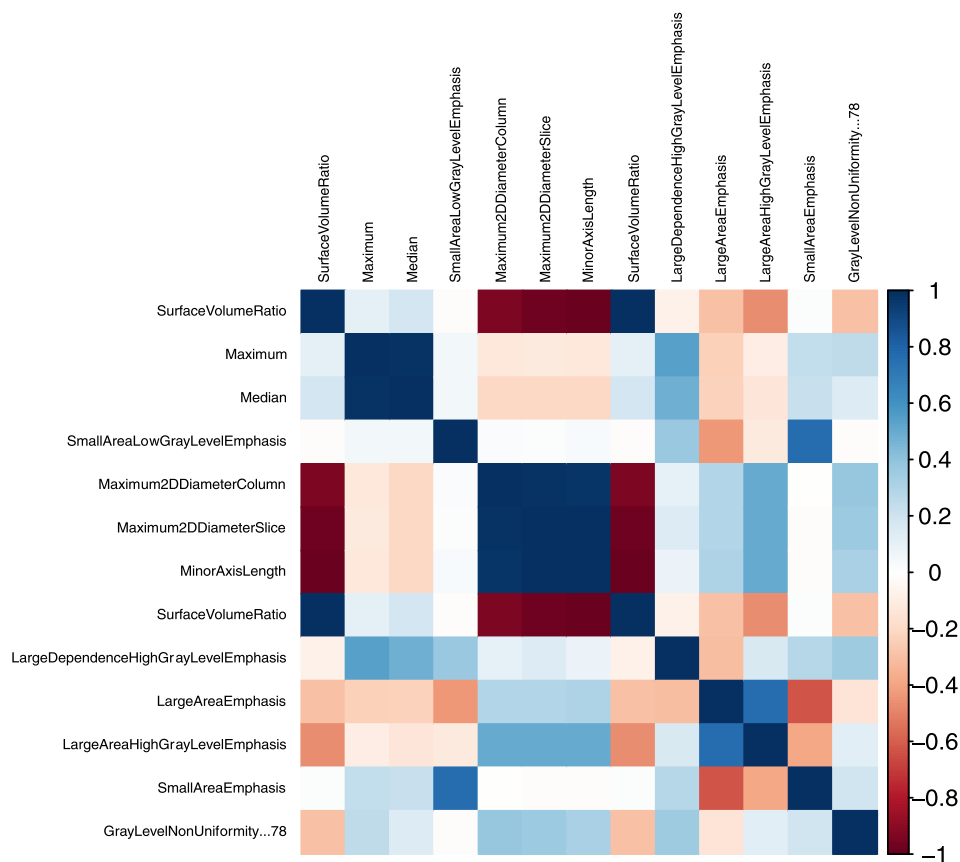


**FIGURE 3** | Correlation matrix of the most important features. GLCM, gray-level co-occurrence matrix; GLDM, gray-level dependence matrix; GLRLM, gray-level run length matrix; GLSZM, gray-level size zone matrix; MCC, maximal correlation coefficient; NGTDM, neighboring gray tone difference matrix.

**TABLE 2** | Illustration of the key radiomics features.

Features
Surface volume ratio
Maximum
Small area low gray level emphasis
Maximum 2D diameter column
Large dependence high gray level emphasis
Large area emphasis
Large area high gray level emphasis
Gray level nonuniformity

may not be visibly apparent. This advanced technique enables us to extract extensive information from image data beyond what is visible to the naked eye [31]. Therefore, in our study, we developed and externally validated a radiomics-derived ML model for staging liver fibrosis MRI images. This study highlights the effectiveness of integrating MRI data with a radiomics-based machine learning classifier for accurately classifying patients with liver fibrosis.

Previous studies developed an ML model for diagnosing various stages of LF using pre-contrast, arterial, portal vein phase,

and three-phase CT images, demonstrating acceptable efficacy in LF assessment [30, 31]. Furthermore, they suggested that the ML model based on the pre-contrast phase might suffice for predicting LF compared with models relying on enhanced CT images [32].

In the context of MRI, a recent study aimed at the automatic staging of hepatic fibrosis in patients with hepatitis B utilized gadolinium ethoxybenzyl diethylenetriamine pentaacetic acid (Gd-EOB-DTPA)-enhanced magnetic resonance imaging with dynamic radiomics analysis, achieving strong classification performance for fibrosis stages [33].

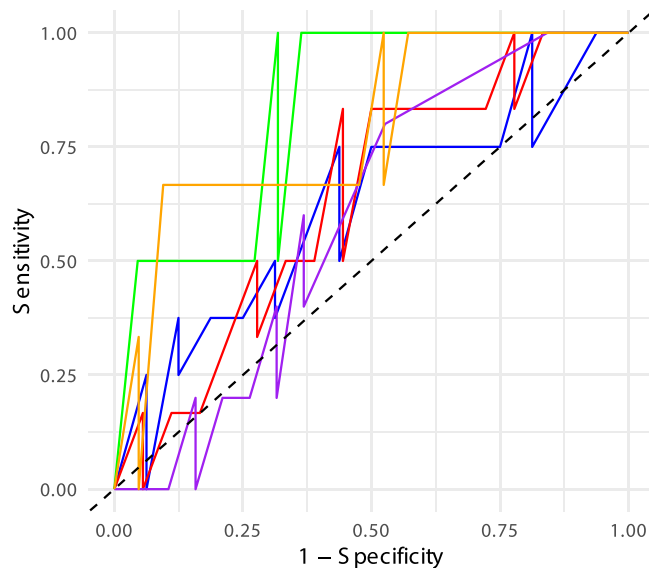
Other recent studies have compared radiomics models with fusion models, which integrate radiomics features with serum fibrosis biomarkers based on MRI images for staging LF in patients with chronic liver disease. These studies specifically determined ROIs within the right hepatic lobe [34]. All these radiomics model demonstrate the potential for highly accurate automatic staging of hepatic fibrosis [33–35].

Our model with automatic complete segmentation of the liver showed the best results in classifying patients into fibrosis grade 2 with an AUC of 0.830 (95% CI 0.520–0.830). As fibrosis grade 2 represents an early stage of liver disease, detecting it through noninvasive methods like radiomics allows for timely intervention. With the application of novel therapeutic approaches for nonfatty liver diseases, early detection enables proactive

**TABLE 3** | Performance of the radiomics model adding ADC-values.

Variables	AUC (radiomics)	AUC (95% CI)	AUC (radiomics and ADC)	AUC (95% CI)	$\Delta$ AUC	<i>p</i>
Fibrosis grade 0	0.617	0.362–0.627	0.454	0.180–0.454	0.163	0.093
Fibrosis grade 1	0.634	0.381–0.634	0.569	0.264–0.569	0.065	0.520
Fibrosis grade 2	0.830	0.520–0.830	0.694	0.375–0.694	0.136	0.230
Fibrosis grade 3	0.610	0.363–0.610	0.700	0.479–0.700	−0.009	0.287
Fibrosis grade 4	0.790	0.463–0.790	0.522	0.090–0.522	0.268	0.052

Abbreviations: ADC, apparent diffusion coefficient; AUC, area under the curve; CI, confidence interval.

**FIGURE 4** | ROC analysis. The ROC analysis indicates the sensitivity and specificity of the gradient-boosted tree trained on the selected most important radiomic features. Blue = 0, red = 1, green = 2, violet = 3, orange = 4 [16]. ROC, receiver operating characteristic.

treatment, potentially preventing disease progression to more severe stages and reducing the need for invasive procedures like liver biopsy [36]. Another advantage is that our ML model can be applied to routine CT or MRI images, providing high reproducibility and accessibility, especially in settings without specialized elastography equipment.

Integrating ADC with radiomics did not consistently enhance the predictive performance for fibrosis grading. While fibrosis grade 3 showed a trend towards improvement in AUC with the addition of ADC, the changes across all grades were not statistically significant, indicating that ADC may not provide substantial added value for fibrosis prediction in this context. Nonetheless, further investigations involving larger patient cohorts are necessary to validate the ML model's efficacy, understand the conditions under which ADC may be beneficial and explore other imaging parameters that could improve fibrosis prediction.

However, our study recognizes several limitations that warrant attention. First, it was conducted intentionally at a single

center, aiming to reduce variabilities linked with scanners from different manufacturers or generations. Second, our study cohort's distribution of liver fibrosis stages was unbalanced. Third, we did not employ advanced methods such as deep learning in this study. Indeed, deep learning holds promise, but comprehending the decision-making processes of these models can be complex and challenging [37, 38]. Despite the high AUC values indicating our gradient boosted tree model's strong discriminatory ability, several limitations suggest potential overfitting. A noticeable issue is the discrepancy between the high AUC values and the low sensitivity for specific fibrosis grades, mainly grades 0, 1, and 3. This discrepancy indicates potential overfitting to the training data, which could result in poorer generalizability when applied to new, independent datasets. Additionally, a possible imbalance in the dataset, where specific fibrosis grades were overrepresented, may have led to suboptimal model performance for the less frequent classes. Furthermore, a limitation of our study is the exclusive use of 1.5 Tesla imaging. Currently, there are limited data on the differences in fibrosis grading accuracy when comparing 1.5 Tesla with higher-field strengths, such as 3 Tesla or even 7 Tesla imaging. Future research is needed to investigate whether these higher-field strengths could provide better resolution or accuracy in fibrosis assessment. Another limitation of our study is the inclusion of healthy volunteers as a control group, assuming them to have fibrosis stage F0. As these individuals did not undergo liver biopsy for confirmation, there is a potential risk of misclassification, which may affect the reliability of our comparisons and the overall findings.

In conclusion, our study highlights the promising potential of utilizing radiomics analysis on MRI imaging for the noninvasive staging of liver fibrosis. This approach offers valuable insights into the tissue characteristics and patterns that could aid in accurately assessing liver fibrosis severity, thereby informing treatment decisions and patient management strategies.

#### Author Contributions

All authors have contributed significantly to this work, participating in the conception, design, analysis, interpretation of data, and writing/editing of this manuscript. J.G. and V.K. wrote the manuscript and designed the research. The other authors were involved in the analysis of the data and performed research. All authors revised the manuscript.

## Acknowledgments

The authors have nothing to report. Open Access funding enabled and organized by Projekt DEAL.

## Ethics Statement

Institutional Review Board approval was obtained.

## Conflicts of Interest

C.B. received speaking fees from Siemens Healthineers. The other authors have no potential conflict of interest to disclose.

## Data Availability Statement

The data supporting the findings of this study are available from the corresponding author upon reasonable request. Due to privacy and ethical restrictions, access to patient data is limited to ensure confidentiality.

## References

1. Z. Younossi, Q. Anstee, M. Marietti, et al., “Global Burden of NAFLD and NASH: Trends, Predictions, Risk Factors and Prevention,” *Nature Reviews. Gastroenterology & Hepatology* 15, no. 1 (2018): 11–20, <https://doi.org/10.1038/nrgastro.2017.109>.
2. S. Petta, V. di, R. Pipitone, et al., “Prevalence and Severity of Non-alcoholic Fatty Liver Disease by Transient Elastography: Genetic and Metabolic Risk Factors in a General Population,” *Liver International* 38, no. 11 (2018): 2060–2068, <https://doi.org/10.1111/liv.13743>.
3. S. K. Sarin, M. Kumar, M. Eslam, et al., “Liver Diseases in the Asia-Pacific Region: A Lancet Gastroenterology & Hepatology Commission,” *Lancet Gastroenterology y Hepatología* 5, no. 2 (2020): 167–228, [https://doi.org/10.1016/S2468-1253\(19\)30342-5](https://doi.org/10.1016/S2468-1253(19)30342-5).
4. M. Eslam, P. Newsome, S. Sarin, et al., “A New Definition for Metabolic Dysfunction-Associated Fatty Liver Disease: An International Expert Consensus Statement,” *Journal of Hepatology* 73 (2020): 202–209, <https://doi.org/10.1016/j.jhep.2020.03.039>.
5. Y. Huh, Y. J. Cho, and G. E. Nam, “Recent Epidemiology and Risk Factors of Nonalcoholic Fatty Liver Disease,” *Journal of Obesity & Metabolic Syndrome* 31 (2022): 17–27, <https://doi.org/10.7570/jomes202021>.
6. X. Ge, L. Zheng, M. Wang, Y. Du, and J. Jiang, “Prevalence Trends in Non-Alcoholic Fatty Liver Disease at the Global, Regional and National Levels, 1990–2017: A Population-Based Observational Study,” *BMJ Open* 10 (2020): e036663, <https://doi.org/10.1136/bmjopen-2019-036663>.
7. A. J. Sanyal, M. van, J. Clark, et al., “Prospective Study of Outcomes in Adults With Nonalcoholic Fatty Liver Disease,” *New England Journal of Medicine* 385 (2021): 1559–1569, <https://doi.org/10.1056/NEJMoa2029349>.
8. C. Filozof, B. J. Goldstein, R. N. Williams, and A. Sanyal, “Non-Alcoholic Steatohepatitis: Limited Available Treatment Options but Promising Drugs in Development and Recent Progress Towards a Regulatory Approval Pathway,” *Drugs* 75, no. 12 (2015): 1373–1392, <https://doi.org/10.1007/s40265-015-0437-3>.
9. S. A. Harrison, P. Bedossa, C. D. Guy, et al., “A Phase 3, Randomized, Controlled Trial of Resmetirom in NASH With Liver Fibrosis,” *New England Journal of Medicine* 390, no. 6 (2024): 497–509, <https://doi.org/10.1056/NEJMoa2309000>.
10. J. Zeng, J.-G. Fan, and S. M. Francque, “Therapeutic Management of Metabolic Dysfunction Associated Steatotic Liver Disease,” *United European Gastroenterology Journal* 12 (2024): 177–186, <https://doi.org/10.1002/ueg2.12525>.
11. M. A. Tincopa, Q. M. Anstee, and R. Loomba, “New and Emerging Treatments for Metabolic Dysfunction-Associated Steatohepatitis,” *Cell Metabolism* 36 (2024): 912–926, <https://doi.org/10.1016/j.cmet.2024.03.011>.
12. D. C. Rockey, S. H. Caldwell, Z. D. Goodman, R. C. Nelson, A. D. Smith, and American Association for the Study of Liver Diseases, “Liver Biopsy,” *Hepatology* 49 (2009): 1017–1044, <https://doi.org/10.1002/hep.22742>.
13. R. A. Standish, E. Cholongitas, A. Dhillon, A. K. Burroughs, and A. P. Dhillon, “An Appraisal of the Histopathological Assessment of Liver Fibrosis,” *Gut* 55, no. 4 (2006): 569–578, <https://doi.org/10.1136/gut.2005.084475>.
14. M. E. Mayerhoefer, A. Materka, G. Langs, et al., “Introduction to Radiomics,” *Journal of Nuclear Medicine* 61, no. 4 (2020): 488–495, <https://doi.org/10.2967/jnumed.118.222893>.
15. B. Kocak, B. Baessler, R. Cuocolo, N. Mercaldo, and D. P. D. Santos, “Trends and Statistics of Artificial Intelligence and Radiomics Research in Radiology, Nuclear Medicine, and Medical Imaging: Bibliometric Analysis,” *European Radiology* 33, no. 11 (2023): 7542–7555, <https://doi.org/10.1007/s00330-023-09772-0>.
16. V. Koch, J. Gotta, V. Chernyak, et al., “Biomechanical Assessment of Liver Integrity: Prospective Evaluation of Mechanical Versus Acoustic MR Elastography,” *Journal of Magnetic Resonance Imaging* (2024), <https://doi.org/10.1002/jmri.29560>.
17. Z. D. Goodman, “Grading and Staging Systems for Inflammation and Fibrosis in Chronic Liver Diseases,” *Journal of Hepatology* 47 (2007): 598–607, <https://doi.org/10.1016/j.jhep.2007.07.006>.
18. A. Fedorov, R. Beichel, J. Kalpathy-Cramer, et al., “3D Slicer as an image computing platform for the Quantitative Imaging Network,” *Magnetic Resonance Imaging* 30 (2012): 1323–1341, <https://doi.org/10.1016/j.mri.2012.05.001>.
19. B. Kocak, B. Baessler, S. Bakas, et al., “CheckList for Evaluation of Radiomics Research (CLEAR): A Step-By-Step Reporting Guideline for Authors and Reviewers Endorsed by ESR and EuSoMII,” *Insights Into Imaging* 14 (2023): 75, <https://doi.org/10.1186/s13244-023-01415-8>.
20. M. B. Kursa and W. R. Rudnicki, “Feature Selection With the Boruta Package,” *Journal of Statistical Software* 36, no. 11 (2010): 1–13, <https://doi.org/10.18637/jss.v036.i11>.
21. E. E. Powell, V. W.-S. Wong, and M. Rinella, “Non-alcoholic Fatty Liver Disease,” *Lancet* 397 (2021): 2212–2224, [https://doi.org/10.1016/S0140-6736\(20\)32511-3](https://doi.org/10.1016/S0140-6736(20)32511-3).
22. S. Singh, A. M. Allen, Z. Wang, L. J. Prokop, M. H. Murad, and R. Loomba, “Fibrosis Progression in Nonalcoholic Fatty Liver vs Nonalcoholic Steatohepatitis: A Systematic Review and Meta-Analysis of Paired-Biopsy Studies,” *Clinical Gastroenterology and Hepatology* 13 (2015): 643–quiz e39–40–654.e9, <https://doi.org/10.1016/j.cgh.2014.04.014>.
23. S. D. Serai and M. Yin, “MR Elastography of the Abdomen: Basic Concepts,” *Methods in Molecular Biology* 2216 (2021): 301–323, [https://doi.org/10.1007/978-1-0716-0978-1\\_18](https://doi.org/10.1007/978-1-0716-0978-1_18).
24. H. E. Akkaya, A. Erden, D. K. Öz, S. Ünal, and İ. Erden, “Magnetic Resonance Elastography: Basic Principles, Technique, and Clinical Applications in the Liver,” *Diagnostic and Interventional Radiology* 24, no. 6 (2018): 328–335, <https://doi.org/10.5152/dir.2018.18186>.
25. M. Nouredin, J. Lam, M. Peterson, et al., “Utility of Magnetic Resonance Imaging Versus Histology for Quantifying Changes in Liver Fat in Nonalcoholic Fatty Liver Disease Trials,” *Hepatology* 58 (2013): 1930–1940, <https://doi.org/10.1002/hep.26455>.
26. F. F. Guglielmo, S. K. Venkatesh, and D. G. Mitchell, “Liver MR Elastography Technique and Image Interpretation: Pearls and Pitfalls,” *Radiographics* 39, no. 7 (2019): 1983–2002, <https://doi.org/10.1148/rg.2019190034>.
27. L. Xi, H. Kang, M. Deng, et al., “A Machine Learning Model for Diagnosing Acute Pulmonary Embolism and Comparison With Wells Score, Revised Geneva Score, and Years Algorithm,” *Chinese Medical Journal* 137 (2023): 676–682, <https://doi.org/10.1097/CM9.0000000000002837>.



28. G. S. Handelman, H. K. Kok, R. V. Chandra, A. H. Razavi, M. J. Lee, and H. Asadi, “eDoctor: Machine Learning and the Future of Medicine,” *Journal of Internal Medicine* 284 (2018): 603–619, <https://doi.org/10.1111/joim.12822>.
29. M. P. Than, J. Pickering, Y. Sandoval, et al., “Machine Learning to Predict the Likelihood of Acute Myocardial Infarction,” *Circulation* 140, no. 11 (2019): 899–909, <https://doi.org/10.1161/CIRCULATIONAHA.119.041980>.
30. J. E. van Timmeren, D. Cester, S. Tanadini-Lang, H. Alkadhi, and B. Baessler, “Radiomics in Medical Imaging—“How-To” Guide and Critical Reflection,” *Insights Into Imaging* 11 (2020): 91, <https://doi.org/10.1186/s13244-020-00887-2>.
31. K. J. Lafata, Y. Wang, B. Konkel, F.-F. Yin, and M. R. Bashir, “Radiomics: A Primer on High-Throughput Image Phenotyping,” *Abdominal Imaging* 47, no. 9 (2022): 2986–3002, <https://doi.org/10.1007/s00261-021-03254-x>.
32. E. Cui, W. Long, J. Wu, et al., “Predicting the Stages of Liver Fibrosis With Multiphase CT Radiomics Based on Volumetric Features,” *Abdominal Radiology* 46, no. 8 (2021): 3866–3876, <https://doi.org/10.1007/s00261-021-03051-6>.
33. L. Xiao, H. Zhao, S. Liu, et al., “Staging Liver Fibrosis: Comparison of Radiomics Model and Fusion Model Based on Multiparametric MRI in Patients With Chronic Liver Disease,” *Abdominal Radiology* 49 (2024): 1165–1174, <https://doi.org/10.1007/s00261-023-04142-2>.
34. M. El-Kassas and K. Alswat, “Editorial: Emerging Therapeutic Approaches for Non-Alcoholic Fatty Liver Disease,” *Frontiers in Medicine* 11 (2024): 1437385, <https://doi.org/10.3389/fmed.2024.1437385>.
35. J. Wang, S. Tang, Y. Mao, et al., “Radiomics Analysis of Contrast-Enhanced CT for Staging Liver Fibrosis: An Update for Image Biomarker,” *Hepatology International* 16 (2022): 627–639, <https://doi.org/10.1007/s12072-022-10326-7>.
36. K. J. Choi, J. Jang, S. Lee, et al., “Development and Validation of a Deep Learning System for Staging Liver Fibrosis by Using Contrast Agent-Enhanced CT Images in the Liver,” *Radiology* 289 (2018): 688–697, <https://doi.org/10.1148/radiol.2018180763>.
37. P. N. Ramkumar, K. Kunze, H. Haeberle, et al., “Clinical and Research Medical Applications of Artificial Intelligence,” *Arthroscopy* 37 (2021): 1694–1697, <https://doi.org/10.1016/j.arthro.2020.08.009>.
38. L. Rubinger, A. Gazendam, S. Ekhtiari, and M. Bhandari, “Machine Learning and Artificial Intelligence in Research and Healthcare,” *Injury* 54 (2023): S69–S73, <https://doi.org/10.1016/j.injury.2022.01.046>.

### Supporting Information

Additional supporting information can be found online in the Supporting Information section.